Decomposition of the Globular Cluster NGC 6397

for Physics or Astronomy 449

by

Hong Tsui

A THESIS SUBMITTED IN PARTIAL FULFILMENT OF
THE REQUIREMENTS FOR THE DEGREE OF

Bachelor of Science (Hons)

in

The Faculty of Graduate Studies

(Physics & Astronomy)

The University Of British Columbia

(Vancouver, Canada)

April, 2008

Abstract

The kinematics and white dwarf distribution have been studied for the Globular Cluster NGC 6397. The data was obtained from NASA's Hubble Space Telescope in 2005. In particular, we used the images of a field 5' Southeast of the core of NGC 6397 from Advanced Camera for Surveys to conduct our analyses. The first part of the study is about the kinematics of the globular cluster. Isotropy of velocity distribution and cluster rotation have been considered. As anticipated, this relaxed cluster exhibited no strong signs of anisotropy. However, there appears to be some level of rotation. The rotational motion turns out to be $\mu_\alpha \cos(\delta) = 3.88 \pm 1.41\ mas\ yr^{-1}$ and $\mu_\delta = -14.83 \pm 0.58\ mas\ yr^{-1}$. This result is not entirely expected and deserves further investigation in future studies.

The second of the thesis is based on white dwarf populations in the globular cluster and the Galactic Bulge. As a first glance, there appears to be a lacking of white dwarfs at the age of approximately $0.6\ Gyr$. Further investigation reveals this to be statistically insignificant. Through this analysis, another pattern of white dwarf abundance is discovered. There appeared to be much more stars at the age between $0.9 - 2.0\ Gyr$. This could be a manifestation of modeling error. As the final consideration of this thesis, white dwarf candidates in the Galactic Bulge are illustrated. Approximately 10 candidates are found at the most probable location of stars in the Bulge.

The analyses conducted in this thesis set stage for further development in understanding of globular clusters. In particular, the rotation analysis raises curiosity about the dynamics of NGC 6397 in the plane of the sky. Moreover, the velocity distribution analysis confirms properties and theories pertaining to globular clusters.

Table of Contents

List of Tables

List of Figures

Acknowledgement

I would like to thank Dr. Harvey Richer and Dr. Jeremy Heyl for guiding the way through my research. I appreciate the extra time that they have to spend showing me basic analytical tools. I have learned a great deal about astronomical research and methods from them. Moreover, I would like to thank Dr. Heyl for meticulously inserting comments throughout the Monte Carlo simulation program; I regret not being able to make that component a useful part of this thesis.

Chapter 1

Introduction and Background

1.1 Globular Clusters

There are many interesting astronomical objects that would yield insight into the formation, kinematics, and age of our own Milky Way. Star clusters are of particular interest because they are readily observable and consist of hundreds of thousands of stars. Two general classes of clusters exist, essentially differing in age, metal abundance, size, and location within the galaxy.

For this thesis, we are interested in the class of cluster known as globular cluster. The other type of cluster, open cluster, will be briefly described for completeness. Open clusters contain up to several hundred gravitationally bounded stars. The core radius (radius at which the surface brightness is half of its central value) is generally a few parsecs. The stars have small peculiar velocities and a mass-to-light ratio close to unity. These clusters are typically located within 50 pc of the plane of the galaxy, where extinction is the most severe. The average open cluster has an age less than 300 Myr. Their metallicities are very scattered and do not follow the general trend that younger clusters are more metal abundant [25].

Globular clusters (GC) are very different than open clusters in terms of size, location, age and metallicity. These are spherically distributed clusters with much greater stellar density. Their luminosities range from $10^4 L_{Sun}\ to\ 10^6 L_{Sun}$. The core radius is usually less than 1 pc. GCs are more interesting than open clusters because they are amongst the oldest objects in our galaxy. Their metallicities can range from 1/3 to 1/300 of the solar abundance of metals, indicating very old stellar populations. In fact, an accurate modeling of their age would provide a lower limit for the age of the Milky Way. A benefit for studying globular clusters over open clusters is provided by their high galactic latitudes. Their features can be thoroughly observed in optical without too much worry about the dust extinction in the galactic plane. They are roughly spherically distributed around the galaxy and we observe more globular clusters towards the centre of the galaxy than away from it. This means we can get an independent estimate of our present location from the galactic centre just from globular cluster distribution [25].

Trigonometric parallax cannot be used to provide information for the distances to the globular clusters because they are typically a few kilo parsecs away. The best standardized method is to conduct an isochrone fitting on the colour-magnitude diagram (CMD) of the cluster while assuming certain parameters like extinction and metallicitiy.

1.2 Globular Cluster NGC 6397

NGC 6397, located in the constellation Ara, was discovered about 250 years ago by Abbe Nicholas Louis de la Caille. Its right ascension and declination are $17^h 40^m 41^s$ and $-53°40'25"$ [22]. In terms of galactic coordinates, its longitude and latitude are $338.17°$ and $-11.96°$, respectively [22].

The effect of reddening caused by interstellar dust in the direction of NGC 6397 is fairly consistent among various observations. The colour excess values are typically $E(B-V)=0.18$. Through a comparison between field subdwarfs and cluster stars, an $E(B-V)=0.183\pm0.005$ was determined in 2003 [10]. Another source determined the colour excess to be 0.18 [11]. The most recent value was determined using cluster white dwarfs, and it turned out to be $E(F606W-F814W)=0.20\pm0.3$ [28].

The distance of NGC 6397 has been estimated by fitting field subdwarfs to the cluster's main sequence. A true distance modulus of $(m-M)_0=12.13\pm0.15$ was determined using subdwarfs from HIPPARCOS in 1998 [21]. A few years later, a similar technique was used to obtain a value of 12.01 ± 0.08 [10]. The most recent estimate was done using cluster white dwarfs and a value 12.03 ± 0.06 was determined [28].

Another important parameter that is used to quantify star clusters is their metal content. NGC 6397 is a metal-poor cluster, but unfortunately there is no clear agreement for its metallicity. A typical value for [Fe/H] is in the vicinity of -2. Two independent estimates suggest a value of -2.03 ± 0.05 [10] and -2.02 ± 0.07 [17].

Finally, the latest estimate of age of NGC 6397 has been conducted using the cluster white dwarfs [28]. In that particular study, a Monte-Carlo simulation of the white dwarf population was compared to the observed white dwarf cooling sequence. The result is an age of $11.47\pm0.47\ Gyr$ at 95% confidence. If we take NGC 6397 to be amongst the oldest objects in the Milky Way, it would place the epoch of original assembly of the our galaxy at $z=3.1\pm0.6$ [28].

1.3 Thesis Overview and Objectives

There are four primary objectives for this thesis. First objective is to extract information about the velocity distribution in the cluster from proper motion of the stars (Chapter 2). Second objective is to determine the possible rotation in NGC 6397 (Chapter 3). Third objective is to determine the significance of missing the white dwarfs in the cluster. Moreover, the masses of the cluster white dwarfs will be established through fitting of cooling models (Chapter 4). Fourth objective is to determine the possible white dwarf candidates in the galactic Bulge (Chapter 5).

The kinematics (Chapters 2 and 3) will be determined through a series of proper motion analyses using images from the Hubble Space Telescope (HST). It is interesting to note that rotation of globular clusters have only been measured for the line of sight from radial velocities up until 2000 [26]. The unique abilities and resolution of the HST allows astronomers to readily measure the motion in the plane of the sky. For our data, the period between observations is about 10 years with the first epoch data taken by the Wide Field and Planetary Camera 2 (WFPC 2) in 1995. The second epoch was captured by the Advanced Camera for Surveys (ACS) in 2005.

The masses of the white dwarfs in NGC 6397 and the Bulge of the galaxy are determined through white dwarf cooling model fitting. The detail will be provided in Chapters 4 and 5, but the outline will be briefly mentioned. ACS data is used to generate a colour-magnitude diagram of the cluster stars. In particular, we focused our attention to the fainter stars in the lower left region of the CMD, which represent the white dwarfs. Bergeron models, along with correct distant moduli and reddening and extinction coefficients, are used to fit the cluster and Bulge white dwarf branches.

Chapter 2

Isotropy of NGC 6397

2.1 Formation of Globular Clusters

One of the first dynamical models of clusters was introduced by King in 1966. This simple model assumed an isotropic distribution of velocities for all members. Needless to say, it is a good first approximation to understanding stellar kinematics in clusters; however, this oversimplification does not reflect the observed behavior of typical GCs. To understand the origin of anisotropy, it would be necessary to consider the formation process and relaxation of GCs.

At present, the formation of galactic globular clusters is still not completely understood. For a number of years, astronomers believed that GCs are formed during one massive collapse event. However, recent observations from HST on the cluster NGC 2808 provide evidence for multiple collapses, as there are three distinct generations of stars [27]. The current explanation for this observation is that NGC 2808 is not a typical cluster because of its enormous mass. It has more than one million stars in the most recent estimates, whereas typical clusters, like NGC 6397, have a fraction (~1/10 - 2/10) of that. Average clusters only have one stellar generation because the radiation from the first batch of stars would push out the residual gas after the initial collapse. Contrarily, a massive cluster would have a stronger gravitational field to retain the gas and allow for second or even third generation collapses. Another possible explanation is that NGC 2808 is not a genuine globular cluster, but a dwarf galaxy that has been stripped of most of its mass during capture by the Milky Way [27]. This multiple-collapse concept is still open to question and much research needs to be done. For our discussion, we will use the traditional approach of single-collapse to describe the formation of GCs.

Globular clusters are formed during the collapse of a molecular cloud which exceeds the critical mass. Beyond this mass, the gas pressure can no longer overcome the gravitational attraction amongst the gas particles. Potential energy of a sphere of radius *r* filled with gas of density ρ is given by [6]

$$E_p = -\frac{1}{2}\int \rho(\boldsymbol{x})\Phi(\boldsymbol{x})d^3\boldsymbol{x} \approx -\frac{16\pi^2}{15}G\rho^2 r^5. \tag{2.1.1}$$

The kinetic or thermal energy in the same sphere with speed of sound c_s is [6]

$$E_k \approx \frac{c_s^2}{2}\frac{4\pi r^3 \rho}{3}. \tag{2.1.2}$$

If $|E_p| > E_k$, then the cloud's diameter *2r* must exceed the lower limit

$$2r \geq \sqrt{\frac{5}{2\pi}}\sqrt{\frac{c_s^2}{G\rho}} \approx \lambda_J \equiv c_s\sqrt{\frac{\pi}{G\rho}} \tag{2.1.3}$$

where λ_J is known as Jeans length. The mass enclosed within λ_J is simply

$$M_J \equiv \frac{4}{3}\pi\left(\frac{\lambda_J}{2}\right)^3 \rho = \frac{\pi}{6}\lambda_J^3\rho, \tag{2.1.4}$$

where M_J is known as Jeans mass. This is the criterion that must be satisfied in order for the molecular cloud to collapse. Once initiated, a process of cascading fragmentation develops due to irregular overdensities in real molecular clouds. From this model, the ages of the cluster members would be very similar because they are formed during the same collapse. An accepted belief is that globular clusters are generally formed when the galaxy is still very young, making them the oldest objects and the least metal abundant.

One can also generalize the Jeans length and mass equations for collapse of stars into clusters. The same concept is applied, where the gravitational potential energy must exceed the kinetic energy. The only parameter that needs to be adjusted is the speed of sound. Instead of c_s, one would use the average random velocity of stars, v. For example, Jeans length would become

$$\lambda_J = v\sqrt{\frac{\pi}{G\rho}} = 27\ pc\ \left(\frac{v}{1\ km\ s^{-1}}\right)\left(\frac{\rho}{1\ M_{sun}\ cm^{-3}}\right)^{-\frac{1}{2}} \tag{2.1.5}$$

in typical astronomical units. Jeans mass would take the form,

$$M_J = 1.0\cdot 10^4\ M_{sun}\left(\frac{v}{1\ km\ s^{-1}}\right)^3\left(\frac{\rho}{1\ M_{sun}\ pc^{-3}}\right)^{-\frac{1}{2}}. \tag{2.1.6}$$

Regardless of how the cluster is formed, either by collapse of a larger structure or expansion of multiple smaller structures, the initial motions of the particles or stars should be mostly radial [15]. Assuming this to be true, conservation of angular momentum would continue to preserve these radial orbits. This anisotropy due to formation should be slowly erased as gravitational interaction amongst the members smoothes the velocity distribution towards isotropy. The gradual evolution towards isotropy is known as relaxation and will be the focus of the next section.

2.2 Relaxation of Globular Clusters

Relaxation is an important process that occurs to many systems modeled by particles. Particles of air or scent will eventually spread around the room because of random collisions that happen about 10^{11} times per second per particle at room temperature and atmospheric pressure at sea level [25]. These collisions allow the particles to exchange energy and momentum with each other, smoothing out the anisotropic distribution. Similar to this concept, stars within a globular cluster also undergo gravitational interactions that allow the cluster to gradually approach isotropy.

2.2.1 Strong Close Encounters

Strong encounters are defined such that a star, A, approaches very close to another star, B, insofar it completely alters the velocity of star B. To simplify the derivation, we will assume all stars in the cluster to have mass m and random velocity of equal magnitude v. We will also assume other gravitational sources to be negligible compared to the forces involved in the A-B interaction. If A and B are initially far

away, the kinetic energy dominates their potential energy with each other. However, as their separation r decreases, the kinetic and potential energies become comparable to each other. In fact, strong encounter is defined such that their potential energy is greater than or equal to their kinetic energy,

$$\frac{Gm^2}{r} \gtrsim \frac{mv^2}{2}. \tag{2.2.1}$$

This means

$$r \lesssim r_s \equiv \frac{2Gm}{v^2}, \tag{2.2.2}$$

where r_s is called the strong encounter radius [25]. The frequency of such encounters can be calculated by determining the number of stars that would be enclosed by the circle drawn out by the strong encounter radius as the star travels around the cluster. For a star travelling at velocity v for a time t, a strong encounter will occur every time another star is within the volume $\pi r_s^2 vt$ centered on its path. If there are n stars per unit volume and one strong encounter within a time t_s, such that $\pi r_s^2 vt = 1$, then

$$t_s = \frac{v^3}{4\pi G^2 m^2 n} \approx 4 \cdot 10^{12}\ yr \left(\frac{v}{10 km\, s^{-1}}\right)^3 \left(\frac{m}{M_{sun}}\right)^{-2} \left(\frac{n}{1 pc^{-3}}\right)^{-1}, \tag{2.2.3}$$

where t_s is the mean time between strong encounters. In general, the time for such strong encounters in typical regions of galaxies is even longer than the age of the universe. These interactions are only important when discussing the dense cores of globular clusters and galactic nuclei [25].

2.2.2 Weak Distant Encounters

For distant encounters, we assume the forces involved are weak such that the stars only slightly deviate from their original paths after each interaction. This allows for the usage of impulse approximation to calculate the forces that the stars would feel had they not been perturbed. A star of mass m_1 is moving with velocity v approaches a star of mass m_2 within a distance of b (impact parameter). m_1 is originally travelling in a straight line, but m_2 gravitationally attracts m_1 and gives it a slight perpendicular velocity $v_\perp$. If we start measuring the time at closest approach, the perpendicular force is

$$\boldsymbol{F}_\perp = \frac{Gm_1 m_2 b}{(b^2 + v^2 t^2)^{\frac{3}{2}}} = m_1 \frac{dv_\perp}{dt}. \tag{2.2.4}$$

Integrating over time, we obtain

$$\Delta v_\perp = \frac{1}{m_1} \int_{-\infty}^{\infty} \boldsymbol{F}_\perp(t) dt = \frac{2Gm_2}{bv}. \tag{2.2.5}$$

The parallel component of the velocity is not changed through the interaction because the duration of the force accelerating m_1 as it approaches m_2 is the same as it moves away and decelerates from m_2. The deflection angle is thus

$$\alpha = \frac{\Delta v_\perp}{v} = \frac{2Gm_2}{bv^2}. \tag{2.2.6}$$

Because $m_1$is deflected towards m_2 and momentum in the perpendicular direction is conserved, the distance between the stars will decrease. However, in order for the impulse approximation to remain valid, this distance cannot change significantly [25]. In particular, the induced perpendicular velocity $\Delta v_\perp$ must be small compared to the initial approach velocity v. This gives rise to the condition

$$b \gg \frac{2G(m_1+m_2)}{v^2}. \tag{2.2.7}$$

During the passage of the cluster, a star will have many distant weak encounters. Each interaction will change the velocity by an amount $\Delta v_\perp$ in random directions. Provided the directions are random, it is not informative to find $\langle \Delta v_\perp \rangle$ as it will turn out to be zero. We will need to add the squares of $\Delta v_\perp$ and find $\langle \Delta v_\perp^2 \rangle$ instead. Following similar procedures as strong encounters, we want to find out the frequency of weak encounters. In time t, the number of stars m_2 passing m_1 with separation between b and $b + \Delta b$ is the product of number density n and volume $vt \cdot 2\pi b \Delta b$. Next we multiply by $\Delta v_\perp$ in the form of Equation 2.2.5 and integrate over b in order to get $\langle \Delta v_\perp^2 \rangle$ [25],

$$\langle \Delta v_\perp^2 \rangle = \int_{b_{min}}^{b_{max}} nvt \left(\frac{2Gm_2}{bv}\right)^2 2\pi b db = \frac{8\pi G^2 m_2^2 nt}{v} \ln\left(\frac{b_{max}}{b_{min}}\right). \tag{2.2.8}$$

After a time t_{relax} , as $\langle \Delta v_\perp^2 \rangle = v^2$, the expected perpendicular velocity of m_1 has the same magnitude as its original velocity. This means the star has completely lost its original trajectory and is 'smoothed out' by random gravitational interactions. If we define $\Lambda \equiv \left(\frac{b_{max}}{b_{min}}\right)$, we can rewrite the relaxation time

$$t_{relax} = \frac{v^3}{8\pi G^2 m^2 n \ln\Lambda} \approx 2 \cdot \frac{10^9 yr}{\ln\Lambda} \left(\frac{v}{10\ km\ s^{-1}}\right)^3 \left(\frac{m_2}{M_{sun}}\right)^{-2} \left(\frac{n}{10^3\ pc^{-3}}\right)^{-1}. \tag{2.2.9}$$

Now one must define the parameters b_{max} and b_{min}. The exact values are open to question, but in our derivation, b_{min} should not be smaller than r_s and b_{max} should be the maximum size of the system of interest. However, t_{relax} does not heavily depend on these parameters as the ratio will go through a logarithmic operator. Essentially we will arrive at a correct order of magnitude for the relaxation time of a cluster even with compromised values of b_{max} (b_{min} is usually taken to be equal to r_s).

2.2.3 Relaxation of NGC 6397

Besides strong and weak encounters, there are additional interactions that must be considered for the relaxation of a globular cluster. One particular interaction that must be considered is the changes in the Galactic potential in which NGC 6397 exists. The orbit of NGC 6397 has a disk crossing time of approximately 100 Myr [12, 18]. This leads to the possibility of disk shocking to interfere with the relaxation process and cluster dynamics. For typical relaxed clusters, like the NGC 6397, disk shocking is the most important close to the tidal radius, and less significant towards the half mass radius [9].

In regards to isotropic velocity distribution, the essence of the previous discussion lies in the fact that NGC 6397 is a relaxed cluster. The age of the cluster is 11.5 ± 0.5 Gyr [22], whereas the core and half-mass radius relaxation times are 0.079 Myr and 0.29 Gyr, respectively [11]. One can see that relaxation

time decreases towards the centre of the cluster because stellar masses and densities increase. This dependence can also be seen in the functional form of Equation 2.2.3 and 2.2.9. It is worthy to mention that mass segregation has also been observed in NGC 6397 [5, 14]. Mass segregation contributes to faster evolution towards isotropy for the cluster center because it tends to move massive stars towards the core.

2.3 Methods of Observing Anisotropy

Until the dawn of the 21st century, anisotropy of stellar motion in globular clusters has been studied through very crude and inaccurate methods. It is accomplished by comparing radial drop-off that is observed with the theoretical models of varying anisotropy. This technique has a serious flaw insofar there is no guarantee for the models to be correct. The combination of observational error and more important, inadequate dynamical modeling would lead to fairly unreliable results [15]. However, the proper motions provided by Hubble's ACS and WFPC 2 allow astronomers to measure anisotropy directly, without the need for complicated dynamical models.

Previous analysis of anisotropy required radial velocity observations. This means the result is heavily dependent on various geometrical perspectives at different radii of the cluster. The velocities observed for the center of the cluster is almost purely v_r. But as we move out towards the edge of the cluster, a larger component of v_t will contribute to the observed velocity. Moreover, due to the escape velocity of clusters, there is a natural drop-off in $\langle v^2 \rangle_{lineofsig\ ht}$ even in clusters with isotropic velocities [15]. Another flaw with radial velocity studies is that they are very sensitive to the model used to calculate the distribution. All these weaknesses make radial velocity a bad choice for analyzing anisotropy.

Proper motions allow astronomers to compare velocity dispersion in the radial and transverse direction. Although there will be projection problems along the line of sight, this method still provides a much more direct measurement of anisotropy [15]. One possible source of error with proper motion analysis is due to cluster rotation. As one can imagine, a rotating cluster will distort the radial and transverse velocities in the plane of the sky. Along any line of sight, the components of rotation will be added or subtracted to proper motions that are parallel to the cluster equator. In another words, rotation would most severely distort the proper motions near the center of the cluster and less towards the edge. A possible correction for this is to find a dynamical model that would account for the rotation. However, this leads to the same modeling problem as radial velocity studies, but with much less dependence on the particular model.

2.4 Hubble Data

A single field located 5' Southeast of the cluster core is imaged with the ACS for 126 orbits (179.7 ksec) in 2005 [22]. This field is chosen because it has a 60% overlap with pre-existing WFPC 2 images. However, due to the short exposure time of the WFPC 2 images (3.96 and 7.44 ksec in 1994 and 1997), the level of detail is fairly limited compared to the ACS image. The location of the ACS field is depicted in Figure 2.1. The regions traced out by bold lines represent the most recent images. The deep outer field taken by the ACS is represented by the rectangular box. A glance at Figure 2.1 would actually reveal two bolded regions. This is because WFPC 2 was simultaneously exposed during the ACS observations. Coincidentally, these WFPC 2 exposures nicely fall on the core of the cluster with the roll angle of the telescope adjusted [22]. This extra set of data will be useful for determining cluster rotation in Chapter 3.

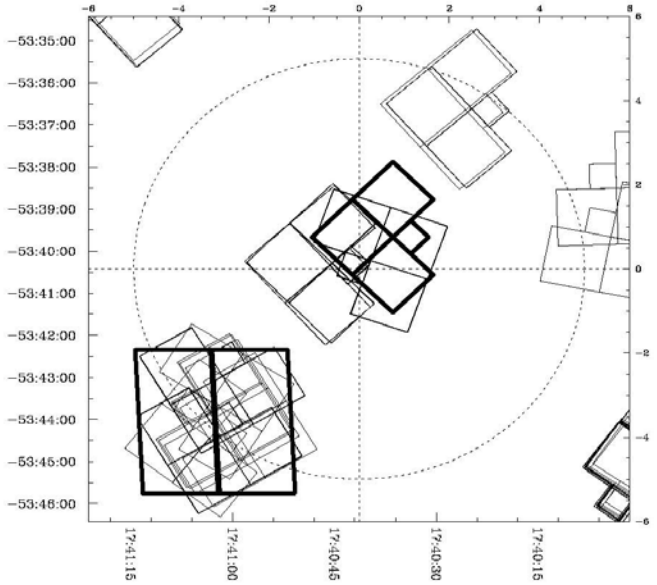

Figure 2.1: Orientation of ACS and WFPC 2 Fields. The horizontal and vertical axes are right ascension and declination, respectively.

The ACS data were reduced by two independent groups at Rice University by J. Anderson and UBC by J. Brewer and H. Richer. We will not go through the details, which can be found in [2, 22] but the selection criteria will be briefly mentioned. In order to eliminate all objects but the stars, all sources with the following properties were removed: (1) noticeably boarder or narrower than a Point Spread Function (PSF), (2) so close in proximity to brighter stars as to be likely PSF artifacts, or (3) on linear features so they were likely to be bumps on diffraction spikes. This reduced the number of objects in the ACS field from 48785 to 8357 true stars [22]. The CMD generated with all 8357 stars is shown in Figure 2.2.

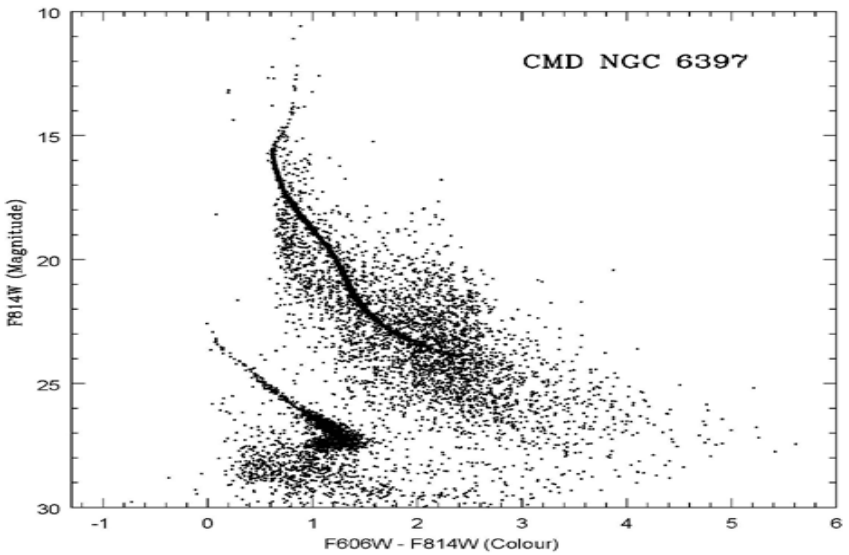

Figure 2.2: CMD of NGC 6397. Distinct main sequence and white dwarf branches can be seen.

2.5 Analysis and Results

We are interested in the velocity distribution of NGC 6397. This equates to finding a method to systematically eliminate all the stars which are not part of the cluster. One solution is to make use of the WFPC 2 images taken in 1994 and 1997. The positions of the stars between the 2005 ACS image and the WFPC 2 images were compared, generating proper motions for the stars within the 60% overlap in areas. Using these proper motions, we can distinguish cluster stars from non-cluster stars because NGC 6397 as a whole has large space motion [22]. The caveat for adapting this method is that we will lose about 40% of the cluster stars due to incomplete overlap of images.

The proper motions were determined such that the zero point is moving with the cluster. Therefore we can isolate the cluster stars by imposing the proper motion condition $dr^2 = dx^2 + dy^2 < 1$. Within the ACS field, 2395 stars meet the proper motion requirement. The proper motion cleaned CMD is shown in Figure 2.3. The result from this reduction procedure is very nice as one can see a very tight main sequence branch and a very distinct white dwarf branch.

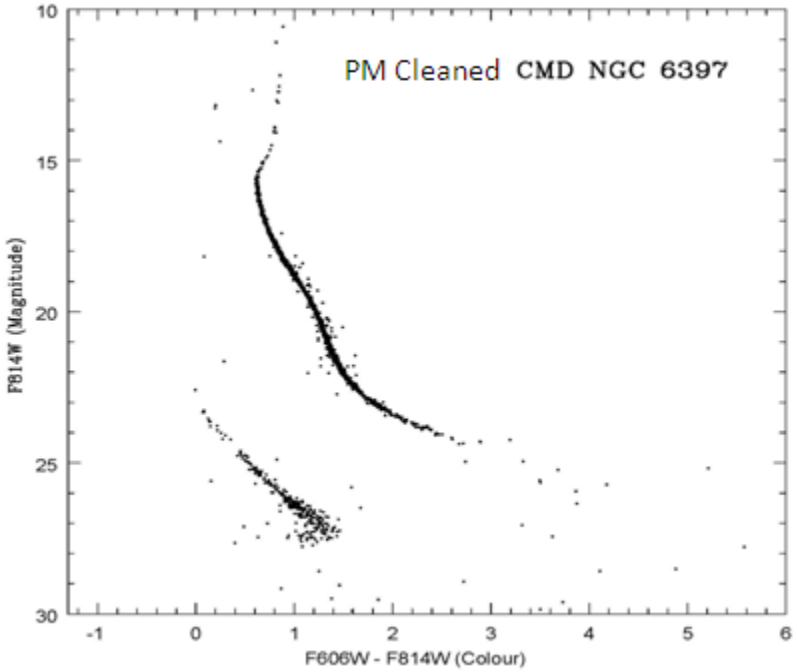

Figure 2.3: Proper Motion Cleaned CMD of NGC 6397. The main sequence and white dwarf branches are much more distinct.

Using the 2395 stars, a distribution of the proper motion directions has been generated. In particular, we have normalized the distribution such that towards the cluster centre is represented by an angle of 0, clockwise rotation is positive, directly away from centre is π, counter clockwise rotation is negative. The geometry is illustrated in Figure 2.4.

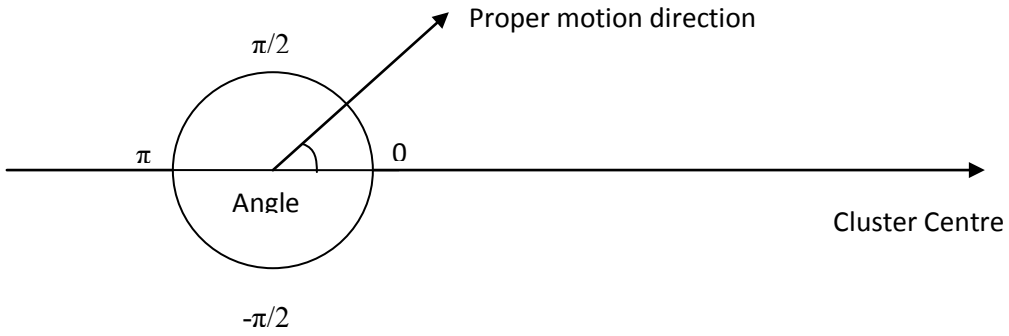

Figure 2.4: Geometry of Proper Motion Normalization.

In order to readily determine the isotropy of the observed distribution, we have plotted the angles against a uniform distribution on a cumulative scale. This is depicted in Figure 2.5. The result is fairly transparent as the two distributions are very similar. To quantify the degree of dissimilarity between the real and uniform distributions, the Kolmogorov-Smirnov test (KS-test) was used. The KS-test, like other statistical tests tries to determine if two datasets differ significantly. However, the KS-test has the advantage of making no underlying assumption about the distribution of data. The level of significance is summarized by the KS value. A large value means the two distributions are alike and a small value means the distributions are distinct. For our analysis, this is the most important property to keep in mind. For a good introduction to the workings of the KS-test, please refer to [16].

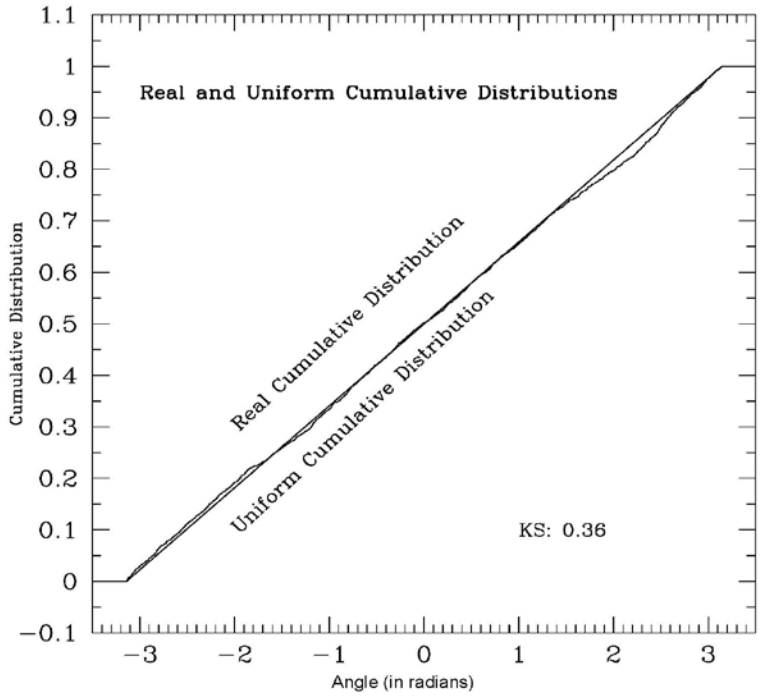

Figure 2.5: Real and Uniform Cumulative Distribution. The KS value between the two distribution is 0.36, indicating a high level of similarity.

From this preliminary analysis, the difference between two distributions is not statistically significant. A KS value of 0.36 is not low enough to draw upon any conclusive statement (for *an*isotropy). Therefore, in hopes to amplify the signal, we have combined the angles and collapsed them into a distribution from 0 to $\pi/2$. First, the clockwise and counterclockwise proper motions are combined. This means we no longer distinguish between the directions of proper motion around the centre. Second, the proper motions directly towards and away from centre are combined. After the two collapses, we can only determine if the proper motions are: (1) moving radially with respect to the cluster centre, or (2) rotating around the cluster centre in the plane of the sky. The idea here is to sacrifice a portion of the directional information in order to amplify the signal. The collapsed distribution is illustrated in Figure 2.6.

The KS value increased as expected. It is now closer to a 2-σ result, indicating some level of distinction between radial and rotational proper motion. If we qualitatively analyze Figure 2.6, three trends can be seen: (1) the two distributions are almost identical between angles 0 to 0.3 radians, (2) there is an overabundance of proper motion between angles of 0.3 to 0.85 radians, and (3) there is an under-abundance or proper motion between angles of 0.85 to 1.4. According to our collapsing scheme, this translates to isotropy in radial orbits but slightly anisotropic rotational orbits around the cluster centre on the plane of the sky. As a side note, due to the nature of cumulative distributions, it is the slopes of lines which determine the relative increase or decrease in abundances, not the absolute position of the lines.

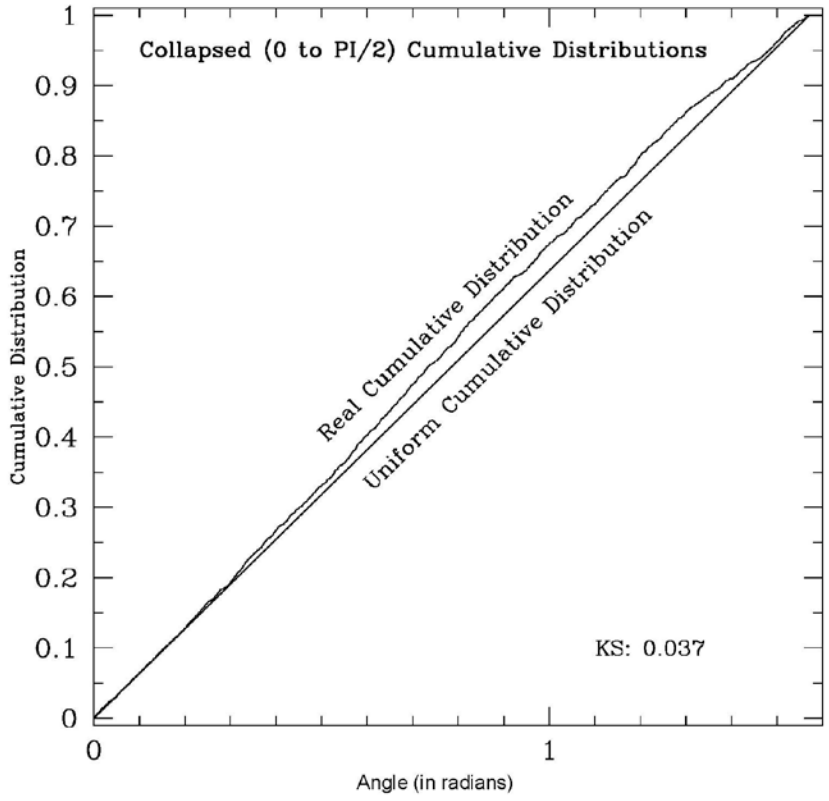

Figure 2.6: Real and Uniform Collapsed Cumulative Distribution. There is observable anisotropy towards the centre of the distributions.

2.6 Conclusion

Observing isotropy in an old, relaxed globular cluster, such as NGC 6397, is an anticipated result. The measured distribution of velocities is very similar to that of a uniform distribution; the resulting KS value is 0.36. Even if the cumulative distributions are collapsed to amplify the signal, the KS value is still only 0.037 (~2σ). The caveat is that some directional information is sacrificed during the collapse, but the signal is still not high enough to determine anisotropy in the cluster as a whole. However, the collapsed distribution yields insight into possible cluster rotation. There are two reasons for this: (1) there seems to be more stars in orbits around the cluster centre in the plane of the sky, and (2) the number of stars travelling towards and away from the cluster centre appears to be fairly similar to the uniform distribution. In other words, there is a good chance for the cluster to be rotating in our line of sight. This peculiarity is the main investigation of the next chapter.

Chapter 3

Rotation of NGC 6397

3.1 Rotation in Globular Clusters

Globular clusters are known to exhibit rotational behavior. The first method for the detection of rotation in GCs dates back in the first half of the 20th century. The main evidence spawned from the observations that showed "flattening" of the spherical structures, implying rotation which compresses the cluster along its spin axis. These ellipticity measurements were first done in the 1920s [23]. Another method for determining rotation in GCs depends on radial velocity measurements of individual cluster stars. Comparing the radial velocity with the star's location within the cluster could provide a lower limit for the degree of rotation of the cluster [8]. The latest method for measuring rotation of globular clusters relies on proper motion of individual stars. Such a study was conducted for the rotation of Globular Cluster 47 Tucanae [23]. It was studied using images taken by WFPC 2, fairly similar to the quality of our images in terms of proper motion. The conclusion was a rotational proper motion of $0.233 \pm 0.055\ mas\ yr^{-1}$. Similar concepts will be used in order to extract rotational information pertaining to NGC 6397.

3.2 Analysis and Results

The space motion of NGC 6397 was studied by [13] very recently using the same set of ACS data obtained in 2005. For details of the data reduction and analysis, please refer to [13]. However, we will mention the most important step in determining an accurate space motion of the cluster. It is to find a set of suitable reference objects. Fortunately, 398 suitable galaxies were found within the ACS field which can be used as references. The potent information from their study to our analysis is the proper motion in the ACS field. The motion is $\mu_\alpha \cos(\delta) = 3.56 \pm 0.04\ mas\ yr^{-1}$ and $\mu_\delta = -17.34 \pm 0.04\ mas\ yr^{-1}$. Figure 3.1 illustrates the distribution of the proper motion.

To determine the rotation of the cluster as a whole, we need to find the absolute motion of the cluster core. This data is provided by the WFPC 2 exposures taken simultaneously with the ACS in 2005. Our method of isolating cluster stars and finding reference objects is not as sophisticated as [13]; nevertheless, it should be provide a good estimate of the rotation NGC 6397 in the plane of the sky.

The first step is to adapt a robust method to isolate cluster stars and field stars using the CMD. There are basically two techniques. One requires the use of proper motion and the other requires the use of the CMD. Isolation of cluster stars in colour space (CMD) turns out to be superior because it does not bias the selected stars. After all, we want to extract proper motion information; therefore it is unreasonable to select stars based on their proper motions in the first place. Figure 3.2 illustrates the groups of stars used to determine the proper motions of the cluster and the field.

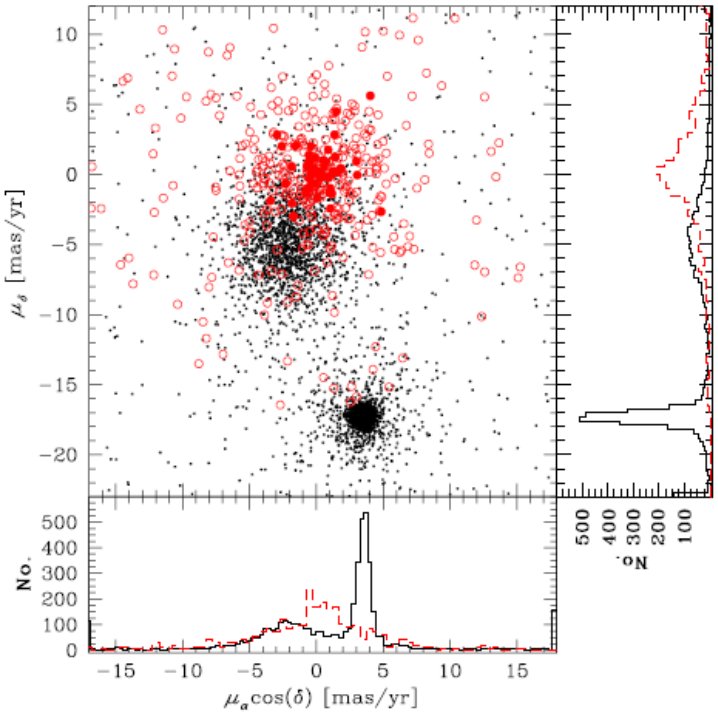

Figure 3.1: Proper Motion of ACS Field: Red dots represent reliable reference objects, in particular, soild red dots and heavily weighted. The 'clump' near the bottom of the plot is the cluster [13].

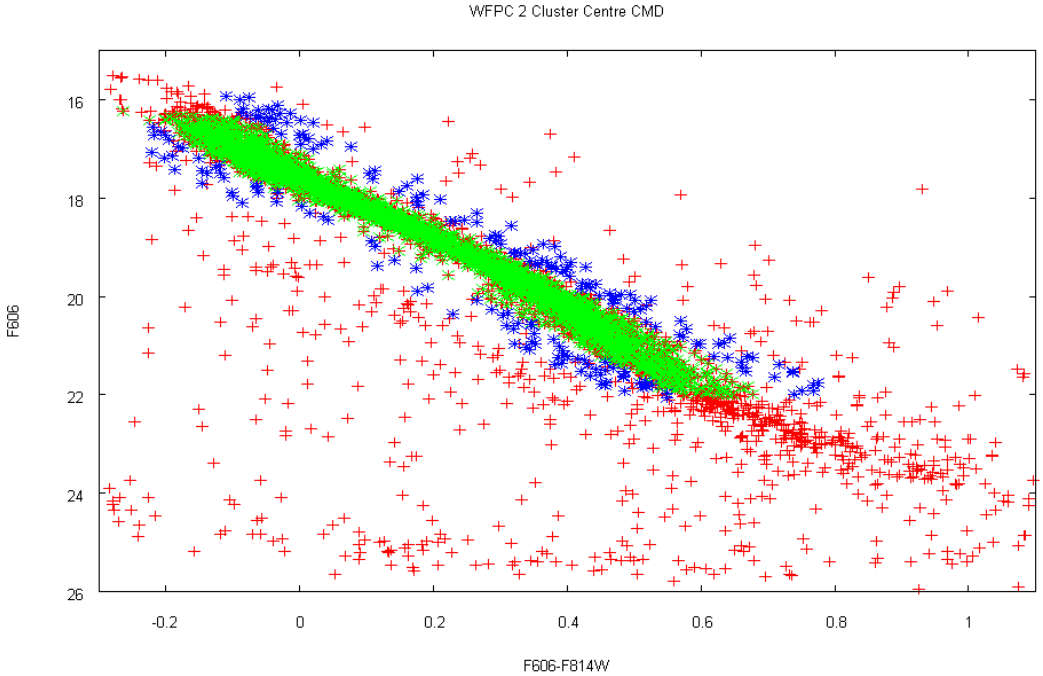

Figure 3.2: WFPC 2 Cluster Centre CMD. The red crosses are all the observed stars. The green and blue crosses are the stars used for calculating proper motions for the cluster and field, respectively. The green crosses represent a large portion of the observed main sequence stars.

It should also be noted that the proper motions are given in units of pixels, so a transformation matrix is used to convert the change in pixel (dx and dy) into $\mu_\alpha \cos(\delta)$ and μ_δ. The transformation has been tested and agrees with the right ascension and declination parameters recorded in the WFPC 2 data set. The values are summarized in Table 3.1.

Cluster Centre Proper Motions ($mas\ yr^{-1}$)	
Cluster Stars	
$\mu_\alpha \cos(\delta)$	2.23 ± 0.13
μ_δ	-1.38 ± 0.06
Field Stars	
$\mu_\alpha \cos(\delta)$	2.55 ± 1.24
μ_δ	1.13 ± 0.48

Table 3.1: Cluster Centre Proper Motions

Using the values from Table 3.1, the proper motion of the cluster stars in the centre of NGC 6397 can be readily determined. It turns out to be $\mu_\alpha \cos(\delta) = -0.32 \pm 1.37\ mas\ yr^{-1}$ and $\mu_\delta = -2.51 \pm 0.54\ mas\ yr^{-1}$. The rotation of the cluster can then be estimated by taking the difference between the values in the centre of the cluster and the values determined in the outer field by [13]. The rotational motion is $\mu_\alpha \cos(\delta) = 3.88 \pm 1.41\ mas\ yr^{-1}$ and $\mu_\delta = -14.83 \pm 0.58\ mas\ yr^{-1}$. This result is not entirely expected because the position of the ACS field is almost directly Southeast of the center. A naïve prediction would presume the direction of the proper motion to be closer to 45° or approximately equal in magnitude for $\mu_\alpha \cos(\delta)$ and μ_δ. Moreover, the direction of $\mu_\alpha \cos(\delta)$ and μ_δ do not correspond to either clockwise or counterclockwise rotation of the cluster in the plane of the sky. A positive $\mu_\alpha \cos(\delta)$ represents motion to the left in Figure 2.1, whereas a negative μ_δ represents motion towards the bottom. This means the estimated proper motion corresponds to stars moving away from the cluster centre. This peculiar proper motion is probably a direct result of not having suitable reference objects.

3.3 Conclusion

Rotation in globular clusters is known to exist. Combining the ACS data (outer field) and WFPC 2 data (inner field), we have generated a rough estimate of the rotation of NGC 6397 in the plane of the sky. The rotational motion at the location of the ACS field (5' SE of cluster centre) is approximately $\mu_\alpha \cos(\delta) = 3.88 \pm 1.41\ mas\ yr^{-1}$ and $\mu_\delta = -14.83 \pm 0.58\ mas\ yr^{-1}$. This result deserves further analysis as we believe the estimate of the proper motion determined from the WFPC 2 data is not very accurate. As a first step, there needs to be a more sophisticated method for identifying reference objects. The two methods we considered, proper motion isolation and CMD isolation, appear to be insufficient for the WFPC 2 data. The first method of proper motion isolation, as discussed in Section 3.2, is biased. The second method of CMD isolation, which we used, does not very accurately distinguish between field stars and cluster stars because the main sequence is not very distinct (Figure 3.2).

Chapter 4

Missing White Dwarfs in NGC 6397

4.1 White Dwarfs

White dwarfs (WD), categorized as class D stars, are a family of stars with mass comparable to the Sun and radius comparable to the Earth. They occupy a region that is below and approximately parallel to main sequence stars on the CMD. The name, white dwarf, is somewhat misleading as it implies the surface colour of the stars to be white. In fact, WDs exist in a large range of colours with temperatures varying from less than 5000 K to more than 80 000 K [6]. There are three subdivisions to WDs according to their spectral type, DA, DB, and DC. The most common form is known as DA white dwarfs which only have pressure-broadened Hydrogen absorption lines. This is the type of WDs that pertains to our analysis.

White dwarfs are burnt out cores of sun-like stars with no nuclear energy source. In particular, we can crudely estimate the pressure at the centre of a WD using [6]

$$P(r) = \frac{2}{3}\pi G\rho^2(R^2 - r^2) \tag{4.1.1}$$

which is derived from hydrostatic equilibrium. Setting ρ and R to typical WD values, we arrive at the pressure at the core of the star to be

$$P(r = 0) \approx 3.8 * 10^{22}\, N\, m^{-2} \tag{4.1.2}$$

We can proceed on to estimating the core temperature assuming this pressure to be true. Using principles of radiative transfer, the change in pressure over the change in radius is related by

$$\frac{dP_{rad}}{dr} = -\frac{\overline{\kappa}\rho}{c} F_{rad} \tag{4.1.3}$$

where $\overline{\kappa}$ is the average opacity and ρ is the density. Using

$$F_{rad} = \frac{L_r}{4\pi r^2} \tag{4.1.4}$$

and

$$P_{rad} = \frac{4}{3}\frac{\sigma}{c}T^4 \tag{4.1.5}$$

which is derived from the Planck function and integrating over energy density, we arrive at the temperature gradient for radiative transport equation,

$$\frac{dT}{dr} = -\frac{3}{4ac}\frac{\overline{\kappa}\rho}{T^3}\frac{L_r}{4\pi r^2} \tag{4.1.6}$$

where $a \equiv \frac{4\sigma}{c} = 7.56591 * 10^{-16} J\, m^{-3} K^{-4}$ is the radiation constant. If we assume the core temperature to be much greater than the surface temperature and set typical WD values for each parameter, Equation 4.1.6 simplifies to

$$T_{core} \approx \left[\frac{3\bar{\kappa}\rho}{4ac}\frac{L_{WD}}{4\pi R_{WD}}\right]^{\frac{1}{4}} \approx 7.6 * 10^7 K \tag{4.1.7}$$

From this crude approximation, one can learn that WDs cannot be composed mainly of hydrogen or else nuclear energy generation would be possible, increasing their luminosities by several orders of magnitude. In other words, the particles in the core of WDs must not undergo nuclear fusion at these densities and temperatures.

4.1.1 Degenerate Matter

Given the extreme densities of WDs, it is possible to show that normal gas and radiation pressure are not sufficient for supporting the structure from gravitational collapse. The mechanism which provides the force required to counteract gravity is a direct manifestation of the Pauli Exclusion Principle (PEP). More specifically, the stellar structure is held up against collapse by electron degeneracy pressure. Combining PEP with Heisenberg's Uncertainty Principle, we arrive at the result

$$P = \frac{(3\pi^2)^{\frac{2}{3}}}{5}\frac{\hbar^2}{m_e}\left[\left(\frac{Z}{A}\right)\frac{\rho}{m_H}\right]^{\frac{5}{3}}, \tag{4.1.8}$$

where Z and A are proton and nucleon numbers, respectively. For full derivation, please refer to [6].

4.1.2 Chandrasekhar Limit

Having derived the electron degeneracy pressure, we can combine it with Equation 4.1.6, and obtain

$$\frac{2}{3}\pi G\rho^2 R_{WD}^2 = \frac{(3\pi^2)^{\frac{2}{3}}}{5}\frac{\hbar^2}{m_e}\left[\left(\frac{Z}{A}\right)\frac{\rho}{m_H}\right]^{\frac{5}{3}}. \tag{4.1.9}$$

Assuming constant density, $\rho = M/\frac{4}{3}\pi R^3$, Equation 4.1.9 becomes

$$R_{WD} \approx \frac{(18\pi)^{\frac{2}{3}}}{10}\frac{\hbar^2}{G m_e M_{WD}^{\frac{1}{3}}}\left[\left(\frac{Z}{A}\right)\frac{\rho}{m_H}\right]^{\frac{5}{3}}. \tag{4.1.10}$$

This result is amazing because it implies $R_{WD} M_{WD}^{\frac{1}{3}}$ is constant or $M_{WD} R_{WD}^3$ is constant. In more 'familiar' terms, more massive WDs are actually smaller than less massive WDs!

However, one can imagine adding more and more mass to an existing WD. What would happen then? Essentially the increasing pressure would increase the velocity of the electrons and eventually they would approach the speed of light. The pressure is now described by

$$P = \frac{(3\pi^2)^{\frac{1}{3}}}{4} \hbar c \left[\left(\frac{Z}{A}\right)\frac{\rho}{m_H}\right]^{\frac{4}{3}}. \tag{4.1.11}$$

If one assumes Z/A = 0.5 for carbon-oxygen WD along with constant density, $\rho = M/\frac{4}{3}\pi R^3$, then combining Equation 4.1.1 with 4.1.11 will provide an estimate of the maximum mass of WDs,

$$M_{Ch} \approx \frac{3\sqrt{2\pi}}{8}\left(\frac{\hbar c}{G}\right)^{\frac{3}{2}}\left[\left(\frac{Z}{A}\right)\frac{1}{m_H}\right]^2 \approx 0.44\, M_{Sun} \tag{4.1.12}$$

A precise derivation of the Chandrasekhar Mass, M_{Ch}, would yield a result of $M_{Ch} = 1.44\, M_{Sun}$. Once again, for full derivation, please refer to [6]. Being able to theoretically derive characteristics of WDs allows us to more confidently establish the mechanisms governing their activities. In particular, no WDs with mass greater than M_{Ch} have ever been found, which supports the concept that electron degeneracy pressure is responsible for maintaining hydrostatic equilibrium in a WD.

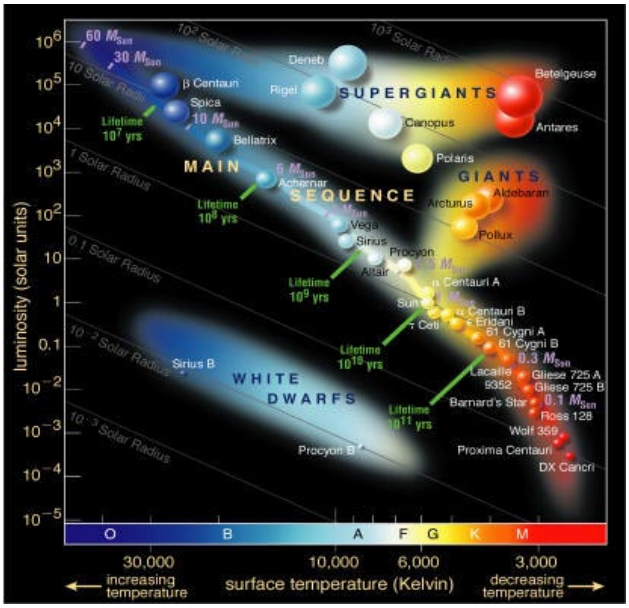

Figure 4.1: Distribution of Star Types in CMD [20].

4.2 Reddening and Extinction

When we look into the sky on a clear night, we see little more than the bright stars luminous enough to transmit their light through all the obstacles that stand between us. In particular, there is aluminous matter which obscure and block out light in our galaxy. This matter is composed of dust and gas particles, which is collectively known as the interstellar medium (ISM). This obscuration due to scattering and absorption of light is referred to as interstellar extinction.

Due to the presence of obscuration, one must modify the distance modulus equation by adding an extra absorption factor,

$$m_\lambda - M_\lambda = 5(\log_{10} d - 1) + a_\lambda \tag{4.2.1}$$

where d is measure in parsec, m_λ and M_λ are the apparent and absolute magnitudes respectively. In addition, this absorption factor should somehow be related to the optical depth. To quantify this, we must combine the simplest form of the radiative transfer equation [6],

$$\frac{I_\lambda}{I_{\lambda,0}} = e^{-\tau_\lambda} \tag{4.2.2}$$

where τ_λ is the optical depth, with the flux-magnitude equation,

$$m_1 - m_2 = -2.5 \log_{10}\left(\frac{F_1}{F_2}\right) \tag{4.2.3}$$

and arrive at

$$m_\lambda - m_{\lambda,0} = -2.5 \log_{10}(e^{-\tau_\lambda}) \approx 1.086\tau_\lambda \tag{4.2.4}$$

where $m_\lambda - m_{\lambda,0}$ is just the change in apparent magnitude due to the obscuration. But we know that is equivalent to the absorption factor according to Equation 4.2.1, therefore

$$a_\lambda \approx 1.086\tau_\lambda \tag{4.2.5}$$

The optical depth through a cloud of dust is simply,

$$\tau_\lambda = \int_0^s n(s)\sigma_\lambda ds \tag{4.2.6}$$

where $n(s)$ and σ_λ are the number density and scattering cross section of the dust particles along the line of sight. Intuitively speaking, absorption should be more severe if there is more dust particles obscuring the light. This can be seen by combining Equations 4.2.5 and 4.2.6.

We can try to qualitatively understand the wavelength dependence of absorption. Dust particles come in a variety of sizes and compositions. One can make a simplifying assumption that each particle is a sphere with radius r and has a scattering cross section of $\sigma_{dust} = \pi r^2$. If the wavelength of light is much larger than the radius of the dust particles, the light passes through the cloud without much extinction. However, if the wavelength is small relative to r, then the light is either completely blocked or severely obscured. A useful analogy to understand this idea would be water waves passing through obstacles. Large objects simply block out the waves whereas small obstacles minutely perturbs the passing waves. This cross sectional analysis was first done by G. von Mie in 1908 [6].

Now that we have a grasp on the wavelength dependence of dust extinction, we can discuss a related concept known as interstellar reddening. As longer wavelengths can more easily pass through a dust cloud, blue light is generally more obscured than red light. For this reason, stars commonly appear redder than their effective temperatures should imply under the influence of dust. Conveniently for astronomers, this is usually not a significant problem because absorption and emission lines in the stars' spectrums can be used to detect this change [6].

4.3 Analysis and Results

Isochrone fitting is commonly used to determine properties of observed stars in a CMD. The model is theoretically developed with certain fixed parameters, for example, masses, ages, and metallicities of the stars. Essentially one would use a variety of models to fit the pattern observed on the CMD. At the end, the characteristics of the stars would be assumed to be most similar to the matching model.

The outline of the procedures taken for our analysis will be summarized in the next few paragraphs. As a first step, a CMD of the WDs in NGC 6397 is plotted using the ACS data, Figure 4.2. Immediately one would see a noticeable gap between 0.35 and 0.40 in the colour axis. The objective of this section is to determine if the gap is statistically significant. In particular, we will convert those magnitudes into ages using the cooling models developed by Bergeron et al. (2006).

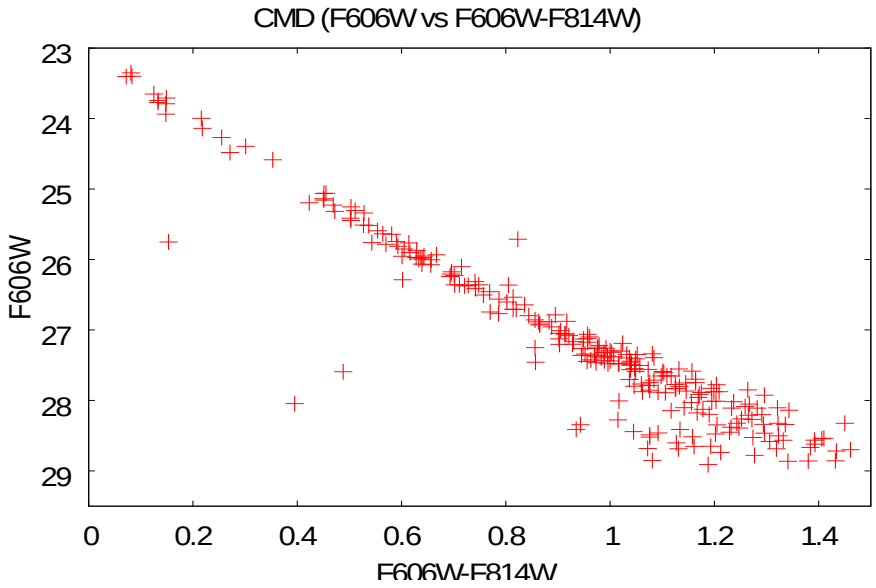

Figure 4.2: Cluster White Dwarf CMD. There is a noticeable gap near the 25^{th} magnitude.

In order to conduct the fitting procedure, the band pass filters for the model and observation must correspond to each other. The ACS data is provided in F606W and F814W filters, whereas the Bergeron models are provided in Johnson UBVRI filters. Figure 4.3 illustrates typical wavelength dependence of the Johnson filters. Figure 4.4 illustrates the F606W and F814W filters specific to the Hubble ACS.

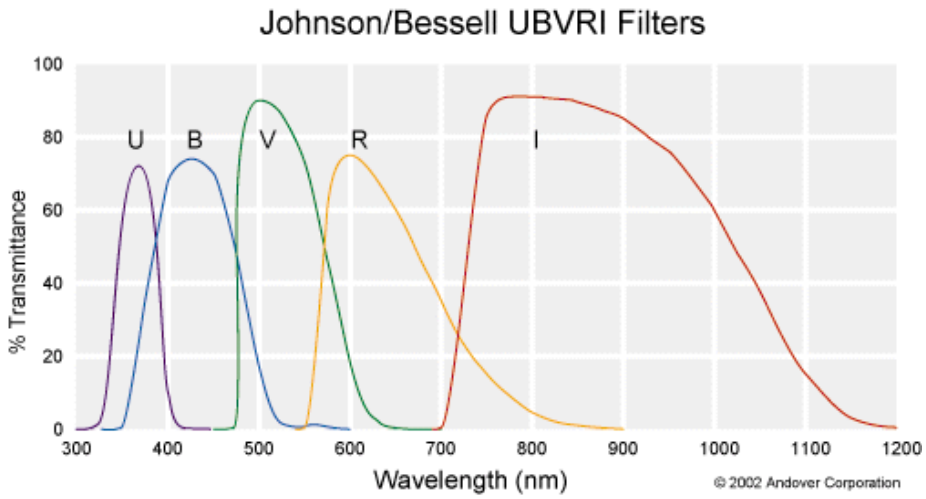

Figure 4.3: Johnson/Bessel UBVRI Filter Characteristics [4].

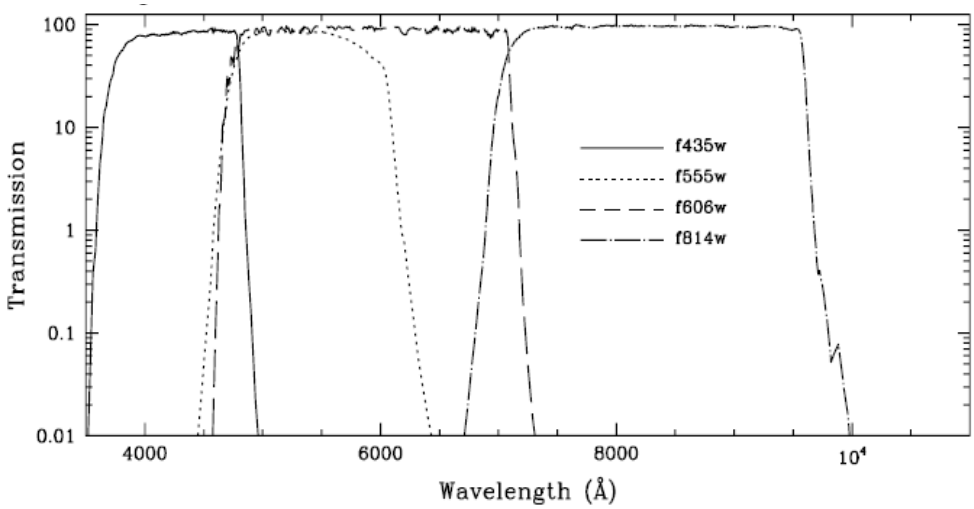

Figure 4.4: WFC Filter Characteristics [1].

The conversion coefficients are summarized in Table 4.1 and 4.2. They are provided by [24]

SOURCE	TARGET		Observed			Synthetic			
SMAG	TMAG	TCOL	c0	c1	c2	c0	c1	c2	TCOL range*
F606W	V	V – I	26.325	0.236	0.000	26.394	0.153	0.096	< 0.4
						26.331	0.340	-0.038	>0.4
F814W	I	V – I	25.495	-0.002	0.000	25.489	0.041	-0.930	<0.1
						25.496	-0.014	0.015	>0.1

*TCOL range applies only to synthetic transformations.

Table 4.1: Coefficients for the Transformation from WFC to BVRI [24].

FILTER	VEGA MAG
F606W	26.398
F814W	25.501

Table 4.2: Synthetic Zeropoints for WFC [24].

As discussed in Section 4.2, interstellar extinction and reddening interfere with the apparent magnitudes that are observed. Fortunately, the extinction and reddening have been previously determined for NGC 6397 [22]. The extinction coefficients are summarized in Table 4.3.

Extinction Coefficient	Value
A_V	0.56
A_I	0.31
$E(V-I)$	0.25

Table 4.3: Extinction Coefficients.

Once the extinction corrections have been applied, the models are converted to F606W and F814W bands. Then the distance modulus of 12.03 ± 0.06, determined by [22], is added to the F606W magnitude. The best fitting Bergeron model is the 0.5 solar mass WDs with pure hydrogen atmospheres (Figure 4.5). Now that we have a working model, a plot of the its age versus magnitude is plotted to observe the dependence (Figure 4.6).

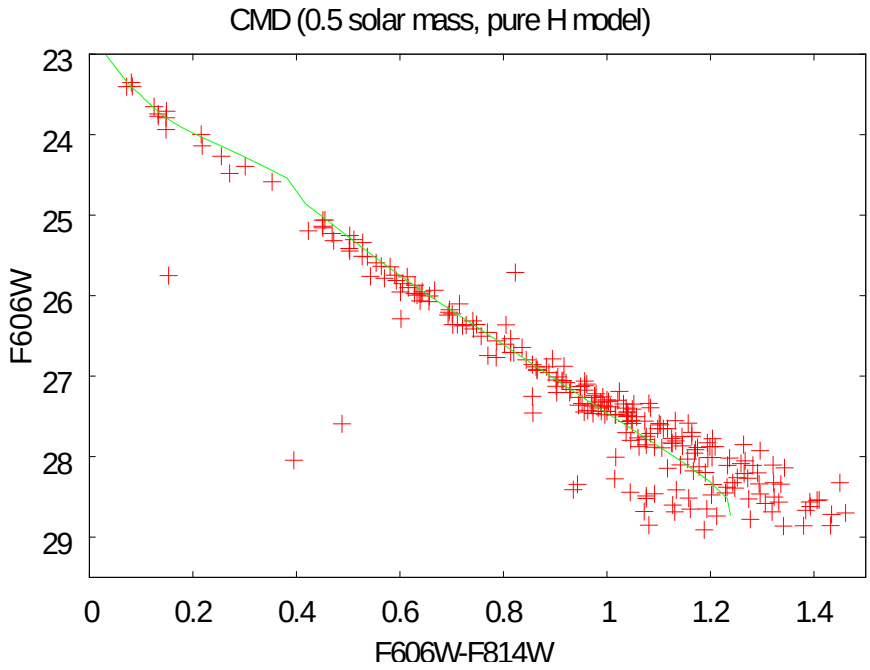

Figure 4.5: Cluster White Dwarf CMD with 0.5 Solar Mass Bergeron Model. The 'kink' near the horizontal position of 0.4 is a result of transformation using the numbers from Table 4.1 and 4.2.

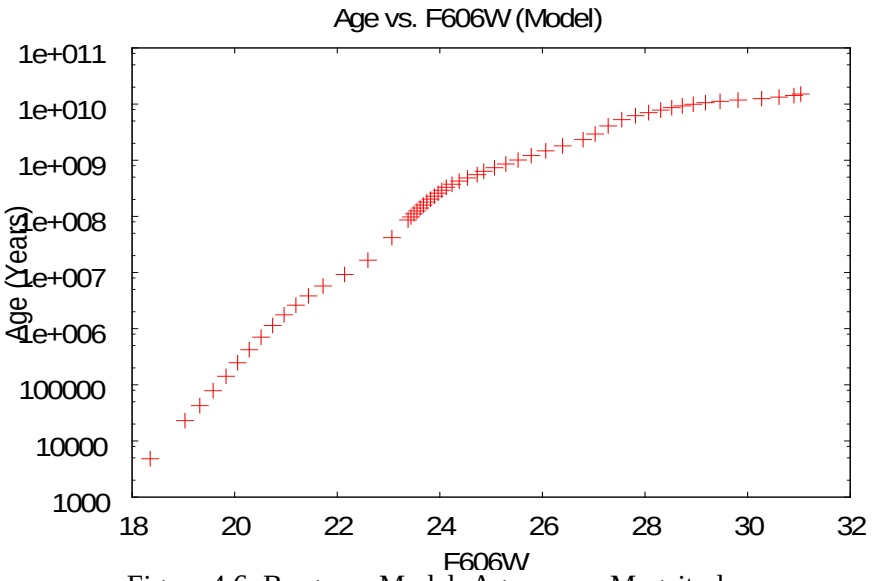

Figure 4.6: Bergeron Model: Age versus Magnitude.

Using the model, we have converted all the stars' magnitudes, down to F606W = 28.5, to age in Gigayears. The distribution is generated and is illustrated in Figure 4.7. One feature that is quickly observable is the over-abundance of white dwarfs between the ages of 1 and 2 Gyr. Moreover, the 'gap' that originally motivated the study turns out to be fairly insignificant. It is located in the 0.6 Gyr bin of the histogram in Figure 4.7.

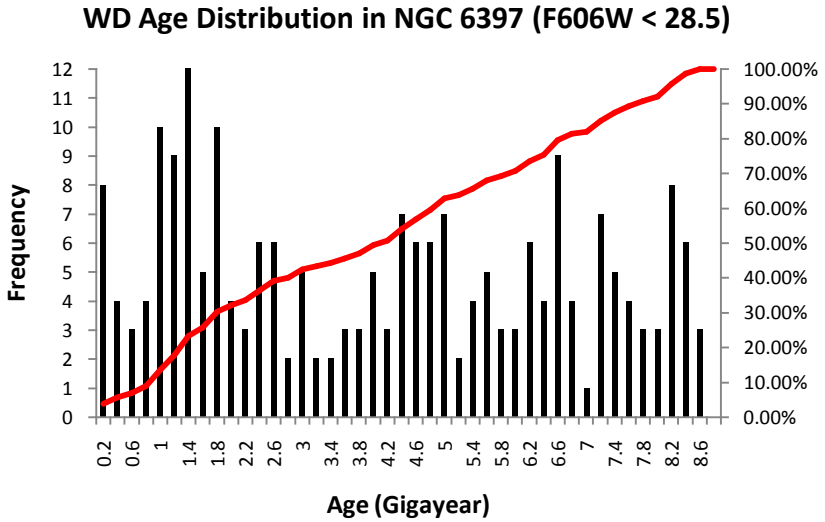

Figure 4.7: White Dwarf Age Distribution in NGC 6397.

Once again, in order to determine the statistical significance, we have conducted a KS test of this distribution against a uniform distribution. The KS value is 0.24, indicating a fair level of similarity between the distributions. The plot of the cumulative distributions are shown in Figure 4.8

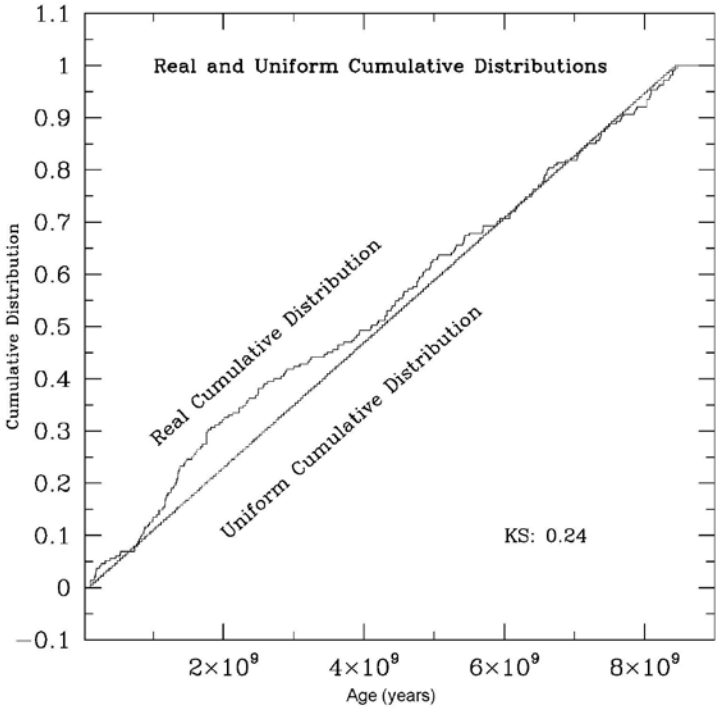

Figure 4.8: Real and Uniform Age Cumulative Distribution.

4.4 Conclusion

The missing white dwarfs, implied by the gap in the CMD (Figure 4.2), in NGC 6397 turn out to be statistically insignificant. In other words, this gap probably does not represent any unusual event that happened in the past leading to an under-abundance of white dwarfs just under the age of 1 Gyr. However, from the cumulative distribution (Figure 4.8), one can see a large deviation from uniformity at the age of 0.9 to 2 Gyr. At 2 Gyr, it slowly settles down to uniformity over the next couple gigayears again. There are two explanations for this observation: (1) approximately 0.9 to 2 Gyr ago, a substantial number of white dwarfs were born, or (2) there appears to be some inaccuracy in the white dwarf modeling. The second explanation is more likely as there is no evidence to suggest why there would be a white dwarf population burst about 1 Gyr ago. However, before stating any conclusions, one should observe that the KS value is merely 0.24. This means the deviation could very well have just happened by chance.

Chapter 5

White Dwarfs in Galactic Bulge

As the final section of this thesis, we will consider the possible white dwarf candidates in the Bulge of the Milky Way. This is possible because the stellar density of NGC 6397 is not high enough to obstruct distant sources in the ACS field.

5.1 Distribution of Starlight in the Milky Way

From observations of other spiral galaxies and data from star counts, distance indicators, abundance analyses and other measurements, astronomers have been able to reconstruct a model of our own galaxy, the Milky Way [6]. The light from spiral galaxies is generally strongest in the near-infrared region of the electromagnetic spectrum, close to 1 μm. This wavelength is commonly emitted by older stars, such as K giants. The reason for this bias in wavelength is because blue light is absorbed by interstellar dust and re-radiated in far-infrared, beyond ~10 μm. However, the optical spectrum is still the most important for determining galactic structure.

The Sun's distance from the center of the galaxy, also known as the Solar Galactocentric Distance (R_0), is recently determined to be $7.62 \pm 0.32\ kpc$ through S2 orbit fits [7]. It is interesting to note that the original estimate by Shapley was closer to $15\ kpc$. The full diameter of the galactic disk is believed to be in the range of 40 to $50\ kpc$ [6].

The galactic disk appears to be composed of three separate components. The young disk probably has a scale height of $50\ pc$. The scale height is defined to be the distance over which the stellar number density drops by 1/e. The young disk is the region where Galactic dust and gas distribution is the most abundant. Another component, the old thin disk, has a larger vertical scale height (z_{thin}), approximately $325\ pc$. The third component, the thick disk, has a scale height (z_{thick}) of $1.4\ kpc$. This disk has much lower stellar density compared to the thin disks. The number density of stars determined from star-count data follows [6],

$$n(z,R) = n_0\left(e^{-\frac{z}{z_{thin}}} + 0.02e^{-\frac{z}{z_{thick}}}\right)e^{-\frac{R}{h_R}}, \tag{5.1.1}$$

where R is the distance from the center of MW, $h_R = 3.5\ kpc$ is the disk scale length, and $n_0 = 0.02$ stars pc^{-3} for the absolute magnitude range $4.5 \leq M_V \leq 9.5$. The Sun is approximately $30\ pc$ above the midplane of the young thin disk. Another important relation to consider is the luminosity density for the old thin disk is,

$$L(R,z) = L_0 e^{-\frac{R}{h_R}}\,\mathrm{sech}^2\left(\frac{z}{z_0}\right) \tag{5.1.2}$$

where $z_0 = 2z_{thin}$ and $L_0 \approx 0.05\ L_{Sun}\ pc^{-3}$. Besides distinguishable stellar densities, the thin and thick disks are also different in terms of their chemical composition and stellar kinematics.

The galactic Bulge was originally thought as a roughly spherical structure near the center of our galaxy. However, observations of Mira variable stars reveal the Bulge to be a bar that is inclined at a particular angle from our line of sight. In another words, it closer resembles an ovular structure from the Sun's point of view. The 'radius' of the Bulge is approximately $1\ kpc$ and has a scale height of $400\ pc$ along the minor axis. The minor axis to major axis ratio is about 0.6.

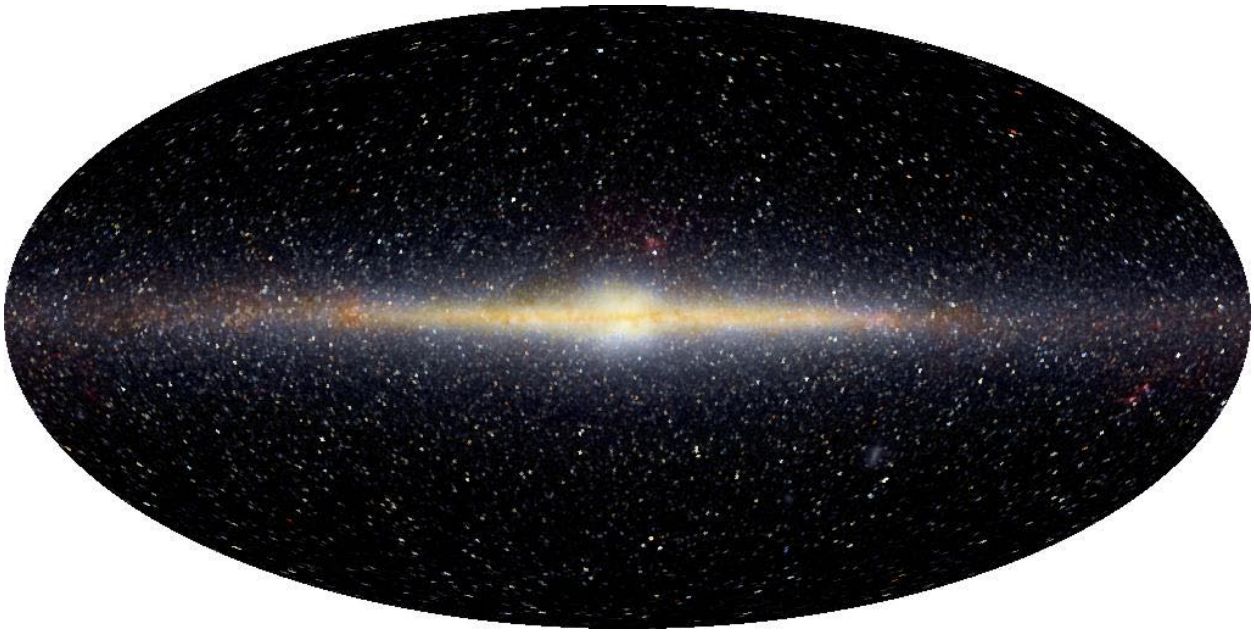

Figure 5.1: COBE View of the Milky Way [19].

5.2 Analysis and Results

Using the CMD generated from the ACS data taken 5' Southeast of NGC 6397, we can see a number of faint field stars dimmer than the cluster white dwarfs. More specifically, we see a branch approximately 2 magnitudes below and parallel to the cluster white dwarfs. This pattern deserves investigation because it can possibly represent white dwarfs in the Galactic Bulge.

If we calculate the most probable distance of the Bulge white dwarfs through basic trigonometry, we arrive at a value of approximately $7.45\ kpc$. Recall from the previous section, the stellar distribution decreases exponentially with radius, so the most probable location is the least distance from the center of the Milky Way. The geometrical setup is illustrated in Figure 5.2. Moreover, the central distribution of gas and dust in our galaxy is located in the midplane (b = 0) of the young thin disk. As we head away from the plane, extinction and reddening effects both decrease. At the location of NGC 6397, the vertical distance from the plane is approximately $0.52\ kpc$. Due to the large distance from the plane, we can make a simplifying assumption. The dust extinction and reddening effects between the Earth and NGC 6397 are approximately equal to the effects between the Earth and the Galactic Bulge.

The distance modulus of NGC 6397 is previously determined to be 12.03 ± 0.03 and the most probable location of the Bulge white dwarfs is approximately $7.45\ kpc$ from our calculation. Using Equation 4.2.1, the distance can be converted to a distance modulus and is approximately 14.36. Taking the difference between these two moduli (Earth-to-6397 and Earth-to-Bulge) would give us an estimate of the decrease in magnitude. The parallel branch approximately 2 magnitudes lower than the cluster WDs is very visible in Figure 5.3.

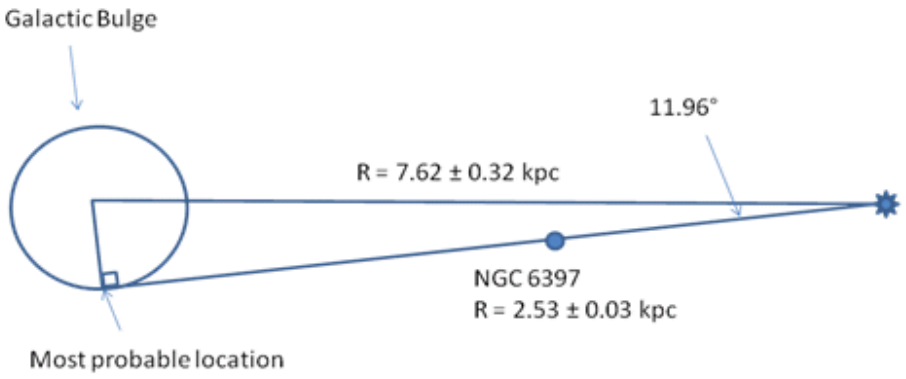

Figure 5.2: Most Probable Location of White Dwarfs in Galactic Bulge

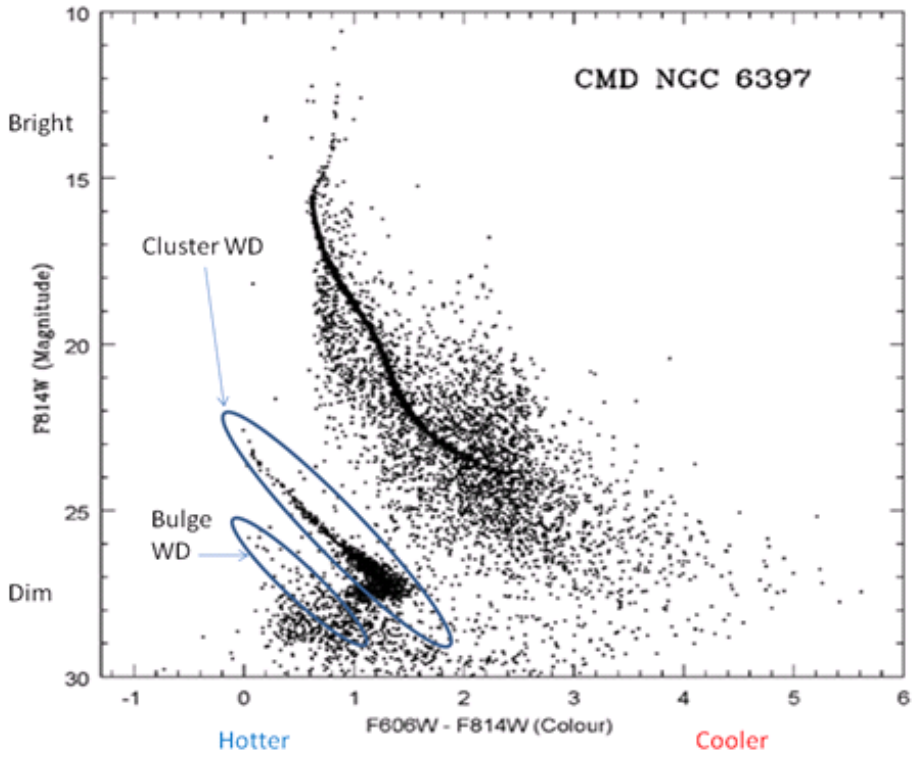

Figure 5.3: CMD of NGC 6397 with White Dwarfs Distinguished.

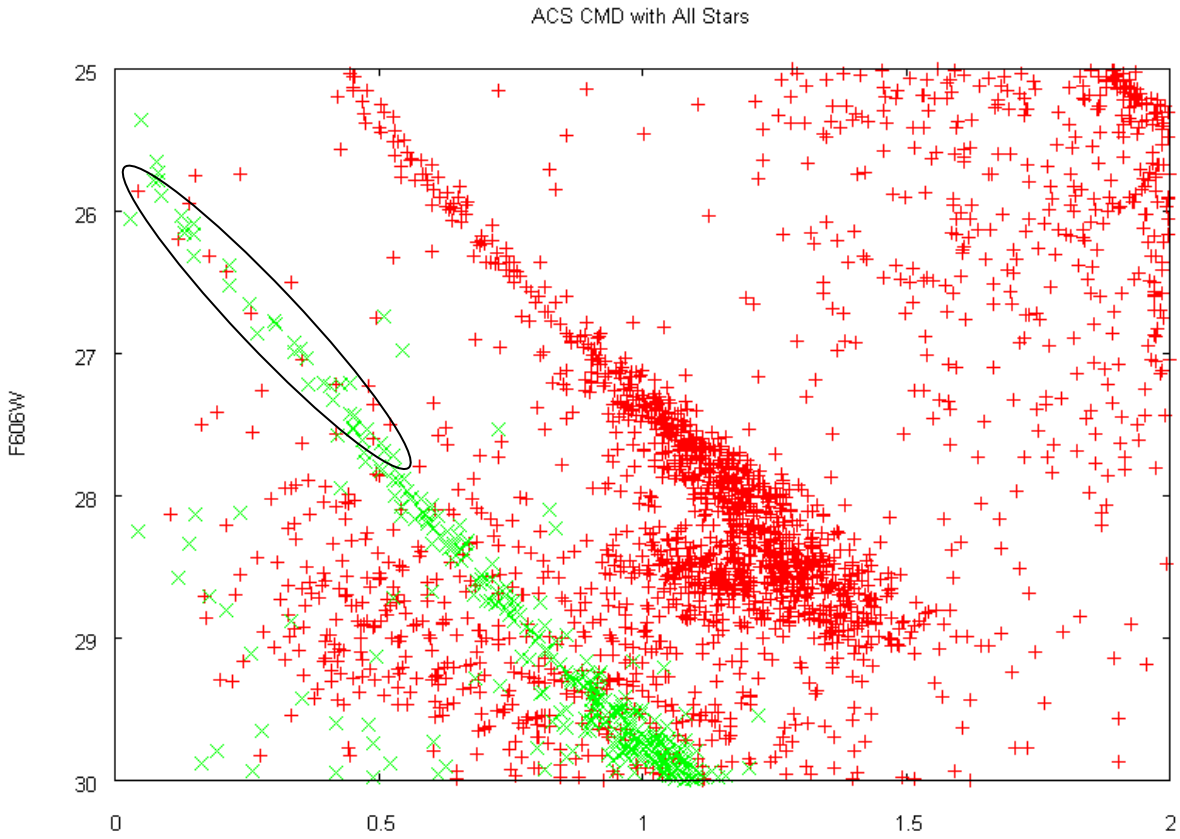

Figure 5.4: Possible White Dwarf Candidates in the Galactic Bulge. The red crosses represent original observations from the ACS. The green crosses are the cluster white dwarfs with an adjustment to the distance modulus corrected for Earth-to-Bulge distance. There is clear overlap in the circled region.

5.3 Conclusion

Through the unparallel capabilities of the ACS onboard the Hubble Space Telescope, we are able to reliably observe the faint stars down beyond ~26 magnitude. This provided the opportunity to study potential white dwarf candidates behind the location of NGC 6397. Making reasonable assumptions about distance modulus and extinction, it is likely that ~10 white dwarfs of 0.5 solar mass are found in the galactic Bulge. This is probably one of the first observations of Bulge white dwarfs, let alone determining their possible masses.

Chapter 6

Conclusions

6.1 Summary and Implication of Results

Using the observations from the Hubble Space Telescope, we have conducted a number of analyses regarding the Globular Cluster NGC 6397. The kinematics of the cluster, including isotropy of velocity distribution and rotation, have been examined. The velocity distribution of roughly 2400 stars in the ACS deep field appears to be virtually uniform. This result is anticipated as relaxed globular clusters are known to evolve towards isotropy. Further analysis of this distribution reveals signs of probable cluster rotation.

Consequently, a rotational study is conducted by comparing motion of the cluster in the outer field with the inner field. The motion at the location of the ACS field (5' SE of cluster centre) is approximately $\mu_\alpha \cos(\delta) = 3.88 \pm 1.41\ mas\ yr^{-1}$ and $\mu_\delta = -14.83 \pm 0.58\ mas\ yr^{-1}$. The result is not entirely expected as the motion does not correspond to clockwise or counterclockwise rotation in the plane of the sky. This result is probably manifested in the method which is used to isolate cluster stars from field stars. In order to arrive at a conclusive result, a more reliable method is necessary for determining reference sources.

The second half of the thesis is pertained to white dwarfs in NGC 6397 and the galactic Bulge. The missing white dwarfs, or 'gap', observed in the CMD of the outer field turns out to be statistically insignificant. The Bergeron cooling models are used to fit the cluster white dwarfs. The best fitting model is the 0.5 solar mass with pure hydrogen atmosphere white dwarfs. After converting the stars' observed magnitudes to ages, a substantial overpopulation of 0.9 to 2.0 Gyr white dwarfs are found. Although the statistical analysis reveal this pattern to be fairly common, there is still reason to believe the cause to be manifested in modeling error.

Finally, potential white dwarf candidates in the Galactic Bulge are studied. After correcting for distance modulus and extinction, there are approximately 10 stars in the Bulge which resembles 0.5 solar mass white dwarfs. This is a pleasant result as few studies have been able to detect white dwarfs in the Bulge.

6.2 Direction for Further Research

The rotation of NGC 6397 in the plane of the sky demands more attention as our preliminary estimates definitely raises curiosity. Better images of the cluster core and more sophisticated methods of identify reference objects would increase the reliability of the rotational proper motion estimates. Another interesting topic would be to study white dwarfs in the Galactic Bulge. If one can accurately determine a sequence of such stars in the centre of the Milky Way, one can learn a phenomenal amount of information about the age and formation of our galaxy.

REFERENCES

[1] Advanced Camera for Surveys Instrument Handbook for Cycle 17, Version 8.0. December 2007. Space Telescope Science Institute. Retrieved from http://www.stsci.edu/hst/acs on March 2008.
[2] Anderson, J., et al. 2008, in preparation.
[3] Anderson, J., King, I. (2003) The Astronomical Journal, 126: 722-777.
[4] Andover Corporation. Retrieved from http://www.andovercorp.com/Web_store/UBVRI/Johnson.php on March 2008.
[5] Andreuzzi, G., Testa, V., Marconi, G., Alcaino, G., Alvarado, F., & Buonanno, R. 2004, A&A, 425, 509.
[6] Carroll B.W., Ostlie D.A. (1996) An Introduction to Modern Astrophysics. Addison-Wesley Publishing Company, Inc.
[7] Eisenhauer et al. (2005). The Astrophysical Journal, 628:246-259.
[8] Ernst, A., Glaschke, P., Fiestas, J., Just, A., Spurzem, R. (2008). N-body Models of Rotating Globular Clusters. Accepted for Publication in the Astronomical Journal. arXiv:0702206v2.
[9] Gnedin, O. Y., Lee, H. M., & Ostriker, J. P. 1999, ApJ, 522, 935.
[10] Gratton, R.G., Bragaglia, A., Carretta, E., Clemintini, G., Desidera, S., Grundahl, F., & Lucatello, S. 2003, A&A, 408, 529
[11] Harris, W.E. 1996, AJ, 112, 1487.
[12] Kalirai, J. S. et al. 2007, astro-ph/0701781.
[13] Kalirai et al. (2008). The Space Motion of the Globular Cluster NGC 6397. arXiv: astro-ph/07017181v2.
[14] King, I. R., Sosin, C., & Cool, A. M. 1995, ApJ, 452, L33.
[15] King, I., Anderson, J. (2000) Dynamics of Star Clusters and the Milky Way. ASP Conference Series, Vol. 000.
[16] Kolmogorov-Smirnov Test. Retrieved from http://www.physics.csbsju.edu/stats/KS-test.html on March 2008.
[17] Kraft, R.P., & Ivans, I.I. 2003, PASP 115, 143.
[18] Milone, A. P., Villanova, S., Bedin, L. R., Piotto, G., Carraro, G., Anderson, J., King, I. R.,& Zaggia, S. 2006, A&A, 456, 517.
[19] NASA. Retrieved from http://map.gsfc.nasa.gov/media/ContentMedia/dirbe123_2p6dec.jpg on March 2008.
[20] Northern Arizona University. Retrieved from http://www4.nau.edu/meteorite/Meteorite/Images/bt2lf1509_a.jpg on March 2008.
[21] Reid, I.N., & Gizis, J.E. 1998, AJ, 116, 2929.
[22] Richer, H., Dotter, A., Hurley, J., Anderson, J., King, I., Davis, S., Fahlman, G., Hansen, B., Kalirai, J., Paust, N., Rich. M., Shara., M, (2008) Deep ACS Imaging in the Globular Cluster NGC 6397: The Cluster Color Magnitude Diagram and Luminosity Function. Accepted for Publication in the Astronomical Journal. arXiv:0708.4030v1.
[23] Shapley H., Star Clusters, McGraw-Hill (1930).
[24] Sirianni et al. (2005). Accepted for publication in PASP. arXiv: astro-ph/0507614v1.
[25] Sparke L.S., Gallagher J.S. (2000) Galaxies in the Universe: An Introduction. Cambridge University Press.
[26] van Leeuwen, F., Le Poole, R. S., Reijns, R. A., Freeman, K. C., & de Zeeuw, P. T. 2000, A&A, 360, 472.
[27] Weaver, D., Villard, R. (2007). Hubble Finds Multiple Stellar 'Baby Booms' in a Globular Cluster. Retrieved from http://hubblesite.org/newscenter/archive/releases/2007/18/full/ March 2008.
[28] Hansen et al. 2007, The White Dwarf Cooling Sequence of NGC 6397. arXiv:astro-ph/0701738v2.